NJC

Pnictogen Bonding with Alkoxide Cages: Which Pnictogen is Best?

Journal:	*New Journal of Chemistry*
Manuscript ID	NJ-ART-07-2019-003648.R1
Article Type:	Paper
Date Submitted by the Author:	12-Aug-2019
Complete List of Authors:	Trubenstein, Henry; Texas Tech University, Chemistry and Biochemistry Moaven, Shiva; Texas Tech University, Chemistry and Biochemistry Vega, Maythe; Texas Tech University, Chemistry and Biochemistry Unruh, Daniel; Texas Tech University, Chemistry and Biochemistry Cozzolino, Anthony; Texas Tech University, Department of Chemistry and Biochemistry

NJC

ARTICLE

Pnictogen Bonding with Alkoxide Cages: Which Pnictogen is Best?

Henry J. Trubenstein,† Shiva Moaven,† Maythe Vega, Daniel K. Unruh and Anthony F. Cozzolino*

0.0Received 00th January 20xx,
Accepted 00th January 20xx

DOI: 10.1039/x0xx00000x

www.rsc.org/

Pnictogen bonding is beginning to emerge as a useful supramolecular interaction. The design strategies for these systems are still in the early stages of development and much attention has been focused on the lighter pnictogens. Pnictogen bond donors can have up to three independent sites for binding which can result in triple pnictogen bonding. This has been observed in the self-assembly of antimony alkoxide cages, but not with the lighter congeners. This work reports structural characterization of an analogous arsenic alkoxide cage that engages in a single pnictogen bond and synthetic explorations of the bismuth congener. DFT calculations are used to evaluate the differences between the structures. Ultimatly, the partial charge on the pnictogen and the energy of the pnictogen lone pair dictate the strength, orientation and number of pnictogen bonds that these cages form. Antimony cages strike the best balance between strength and directionality, allowing them to achieve triple pnictogen bonding where the other congeners do not.

Introduction

A pnictogen bond (PnB), in analogy to a halogen or chalcogen bond (XB/HaB or ChB), is "the net attractive interaction between an electrophilic region associated with a [pnictogen] atom in a molecular entity [the PnB donor] and a nucleophilic region in another, or the same, molecular entity [the PnB acceptor]."[1] Collectively, these interactions are part of a broader class of secondary bonding interactions (SBIs)[2] of the p-block elements (historically also referred to as charge-transfer bonding,[3] donor-acceptor interactions,[4] or closed-shell interactions[5]) which occur despite the formal presence of lone pair of electrons on the electrophilic atom. The PnB length ranges from longer than a single or hypervalent bond to distances around the sum of the van der Waals radii. It should be further elaborated that the formation of a PnB occurs without significant geometric reorganization of the PnB donor, thus differentiating pnictogen bonding from typical Lewis acidic behaviour observed with pnictogens in the +5 oxidation state.

Pnictogen bonding is well-recognized as an important structure directing interaction in the solid state.[6] Interactions that satisfy the above criteria are routinely observed with arsenic,[7–9] antimony[10–14] or bismuth.[15–23] Recently, antimony centred PnBs have been purposefully designed into molecules to actively direct the self-assembly of reversed bilayer vesicles,[24] enable anion binding with applications in sensing and transport,[25–28] self-assembly complex architectures through triple pnictogen bonding[29] and allow for supramolecular catalysis.[30] These applications rely on the predictable formation of PnBs. A useful tool for evaluating this is the map of the electrostatic potential (ESP) onto the electron density. Maxima in the potential (V_{max}) near the van der Waals surface that have large positive values along the elongation of the primary bond are indicators of the ability to form strong interactions. Much like with hydrogen bonding, polar primary bonds tend to maximize the value of the V_{max}. Given that primary bond polarity is a significant predictor of secondary bond strength, it is clear for halogen bonding that iodine (X_p = 2.66) is the correct choice for promoting strong interactions. The trend is also observed with the chalcogens, where the strength of the chalcogen bond increases as the primary bond polarity increases. For the pnictogens (P to Bi), all the electronegativity values are comparable to those of hydrogen. This, to a first approximation, suggests that when these atoms form primary bonds with suitably electronegative atoms, they will have polar primary bonds and participate in pnictogen bonds of similar strength. An additional design criterion with trivalent pnictogens is that there can be up to three independent V_{max} positions and a V_{min} (associated with the lone pair) at the same pnictogen atom.

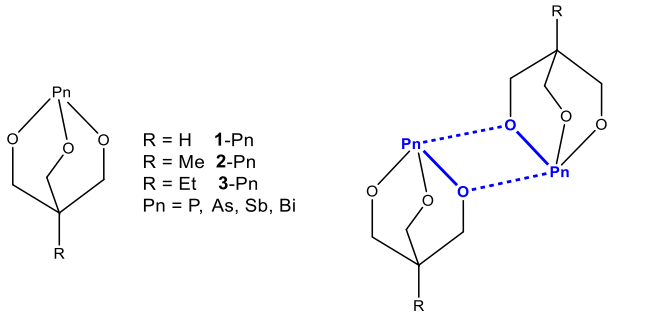

Figure 1. Pnictogen alkoxide cage structures and dimer depicting the $[Pn–O]_2$ supramolecular synthon in blue.

Department of Chemistry & Biochemistry, Texas Tech University, Lubbock, TX 79409, USA. E-mail: anthony.f.cozzolino@ttu.edu.
† These authors contributed equally to the manuscript.
Electronic Supplementary Information (ESI) available: Synthetic and computational procedures, NMR and IR spectra, PXRD patterns. See DOI: 10.1039/x0xx00000x

A previous study on antimony(III) alkoxide cages (Figure 1) revealed that three independent V_{max} sites opposite to three polar primary bonds directed the formation of three strong pnictogen bonds, each with an experimentally estimated energy of 33 kJ/mol.[10] The design was chosen to provide sufficient space around the pnictogen to accommodate the lone pair and the formation of three pnictogen bonds opposite to each of the three polar primary bonds. Based on electronegativity arguments alone, it is expected that the other pnictogen atoms should be able to form strong pnictogen bonds when paired with oxygen; the polarity of the bond between antimony and oxygen should be similar to that of an arsenic oxygen bond. Only one such arsenic alkoxide cage has been crystallographically characterized and it is observed to participate in only one weak PnB.[31] The length of the appended alkyl chain could, perhaps be a contributing factor to the absence of further pnictogen bonds. Pnictogen bonding in the phosphorus congener is rare, and the bismuth analogue has only been studied by elemental analysis.

This study reports the preparation of arsenic alkoxide cages along with spectroscopic and structural characterization. In contrast to antimony, only a single pnictogen bond is observed to form at each arsenic centre. Analogous bismuth alkoxides were prepared using similar approaches. Structural characterization remained elusive, but vibrational spectroscopic studies hint at the possibility of strong pnictogen bonds that prevent solubilization of the product. A detailed DFT study is used to provide insight into this deference as well as explore the trends in pnictogen bonding from P to Bi.

Results and Discussion

Synthesis and Characterization of Arsenic Alkoxide Cages

Arsenic alkoxide cages, **2**-As and **3**-As, were prepared under mild conditions by treating arsenic(III) ethoxide with the appropriate triol (Scheme 1) following a similar procedure used to prepare the analogous antimony cages.[10] Both compounds have been previously reported, preparation of **2**-As by treatment of the triol **4** with $AsCl_3$ and **3**-As by treatment of triol **5** with As_2O_3.[31,32] In contrast to the antimony cages, the arsenic cages did not precipitate out of THF. This higher solubility is at odds with the formation of multiple strong pnictogen bonds.

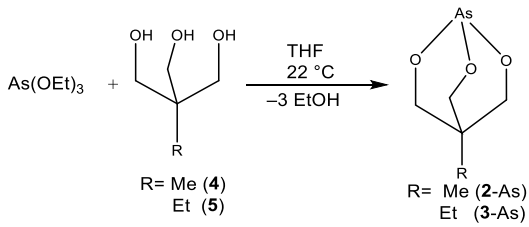

Scheme 1. Synthesis of compounds **2**-As and **3**-As.

Pure materials, established by combustion analysis, were obtained by recrystallization from hexanes. The ^{1}H NMR of both **2**-As and **3**-As revealed a loss of the hydroxyl proton signals along with a marked shift in the resonances of the cage methylene protons. This is consistent with what was observed upon cage formation for the analogous antimony compounds.[10] The FTIR spectrum was consistent with the loss of H from the alcohols as well as the formation of a new As-O bond with stretching frequencies of 583 and 581 cm^{-1} for **2**-As and **3**-As, respectively. These vibrations are found at a lower energy than the corresponding one in the starting compound, $As(OEt)_3$, which absorbs at 604 cm^{-1}. It has been previously noted for antimony compounds, that the vibrational frequencies are affected by the formation of pnictogen bonds.[10,33–35] This can be rationalized by applying an orbital model in which the low-lying σ* orbital of the pnictogen-oxygen primary bond is populated during formation of the pnictogen bond, leading to a weakening of the primary bond. The resulting shift to lower energy in the IR is, therefore, an important spectroscopic signature of pnictogen bond formation. DFT calculations predict vibrational frequencies of 599 cm^{-1} for monomeric **2**-As or **3**-As. Computationally, dimerization through pnictogen bond formation is predicted to shift the vibrational energy to 583 cm^{-1}. This is consistent with the observed experimental stretching frequency and evidence of pnictogen bond formation in the solid state for **2**-As and **3**-As. It is notable that the predicted change in the vibrational frequency is smaller for arsenic (16 cm^{-1}) than was predicted for antimony (47 cm^{-1}). This would be consistent with a much weaker pnictogen bond in the case of As.

Attempted Preparations and Characterizations of Bismuth Congener

Several attempts to prepare **2**-Bi and **3**-Bi using different bismuth starting materials, such as $BiCl_3$, Bi_2O_3, $Bi(O^tBu)_3$, $Bi(NMe_2)_3$, were made. All attempts resulted in the formation of amorphous solids or gels depending on the reactions conditions (for additional details see Table S1 in the SI). Controlling the rate of the reaction, either by slowing down the addition of a base in the case of $BiCl_3$, slow diffusion of reagents together, or addition of a complexing reagents such as Me_6TREN did not facilitate formation of ordered crystalline material. Upon drying, the products were not soluble in common polar organic solvents (such as DMSO, DMF, and pyridine) even at temperatures close to the boiling point of the solvents and therefore could not be characterized by solution methods.

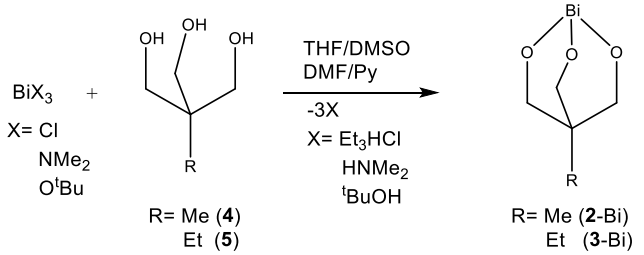

Scheme 2. Synthesis of compounds **2**-Bi and **3**-Bi.

Addition of water to a suspension of **2**-Bi or **3**-Bi (prepared by treatment of the triol with $Bi(NMe_2)_3$) in DMSO-*d*6 allowed for acquisition of a ^{1}H NMR spectrum which revealed signals that

only correspond to the free alcohol, suggesting that they result from the clean hydrolysis of the sample (see figures S6 and S7). The hydrolytic sensitivity is in line with that of the Sb and As compounds. Knowing that the isolated materials are free of organic contaminants allowed for characterization by FTIR. No OH stretch, associated with the free alcohol were observed, indicating that the anticipated alcoholysis of the bismuth amide had occurred. DFT calculated vibrational frequencies for monomeric **1**-Bi predict the C–O stretching band to show up at 1099 cm^{-1}. The same stretching mode in a dimer is predicted to shift to lower energy, 1062/1056 cm^{-1} or 1097 cm^{-1} depending on the antiparallel or orthogonal supramolecular isomers, respectively. Samples of **2**-Bi and **3**-Bi have C–O stretching bands at 1052 cm^{-1} and 1064 cm^{-1}, respectively, which is in agreement with DFT calculations of the aggregated systems (see Table 1). Three Bi–O stretching bands should be expected. DFT calculations on a monomer predict frequencies of 545 cm^{-1} and 531 cm^{-1}. Models of the dimers predict the anticipated red shift following PnB formation. Frequencies of 518 cm^{-1}, 486 cm^{-1}, and 471 cm^{-1} are predicted for the orthogonal dimer and 515 cm^{-1}, 501 cm^{-1}, and 487 cm^{-1} for the antiparallel dimer. The experimental IR results reveal Bi–O stretches that are very similar to those predicted for the dimers (see Table 1). The observed Bi-O stretching frequencies are more than 50 cm^{-1} lower in energy compared to those in $Bi(O^tBu)_3$ (see Table 1) which is known to form pnictogen bonds. The structure is tentatively assigned as the expected cage structure and these results suggest that the bismuth compound that forms is involved in very strong PnBs which is consistent with the observed poor solubility.

Table 1. Computational (grey background) and experimental (white background) vibrational frequencies for bismuth(III) alkoxides.

	ν_{C-O} (cm^{-1})	ν_{Bi-O} (cm^{-1})
$Bi(O^tBu)_3$	1180	568, 559, 551
1-Bi	1099	545, 531, 532
(**1**-Bi)$_2$ ⊥	1056	518, 486,471
(**1**-Bi)$_2$ ‖	1097	515, 501, 487
$Bi(O^tBu)_3$	1176	539
2-Bi	1052	502, 489, 473
3-Bi	1064	505, 493, 469

Structural Characterization Arsenic Alkoxide Cages

Single crystal structures for **2**-As and **3**-As were obtained. In the case of **3**-As,[31] the structure matched with the previously reported structure and in both cases, the powder X-ray diffraction patterns of the bulk materials confirmed that both were a single phase that matched the single crystal structures. Both structures revealed a single molecule in the asymmetric unit with the anticipated cage geometries. The As–O bond lengths are typical (1.769–1.788 Å) for As–O single bonds.[36] The supramolecular arrangements of the two compounds are nearly identical. Each molecule of **2**-As or **3**-As engages in two pnictogen bonds, one as the PnB donor and one as the PnB acceptor, to form a virtual four-membered heterocycle (Figure 1 and Figure 2). This supramolecular synthon is regularly observed between compounds containing heavy pnictogen or chalcogen atoms as they can form SBIs at an ~90° angle to a primary bond.[10,37] This contrasts with hydrogen and halogen bonding, where the monovalency of the hydrogen and halogen atoms restricts secondary bond formation to a position opposite the primary bond. The As···O pnictogen bonds are 2.895(2) and 2.875(1) Å, respectively for **2**-As and **3**-As. These distances are around 156% and 154% of the Σr_{cov}, or 86% and 85% of the Σr_{vdW}[38,39] and are comparatively longer than the analogous Sb···O pnictogen bonds (% of Σr_{vdW} = 67% for **2**-Sb, 77% for **3**-Sb), again suggesting weaker pnictogen bonding for arsenic than antimony.[10] In further contrast, the antimony congeners participate in three distinct PnBs, whereas there is only one PnB per arsenic in the structures of **2**-As and **3**-As. Continuing this trend, there are no apparent pnictogen bonds in the crystal structure of the phosphorus congener, **2**-P (Figure 3).[40]

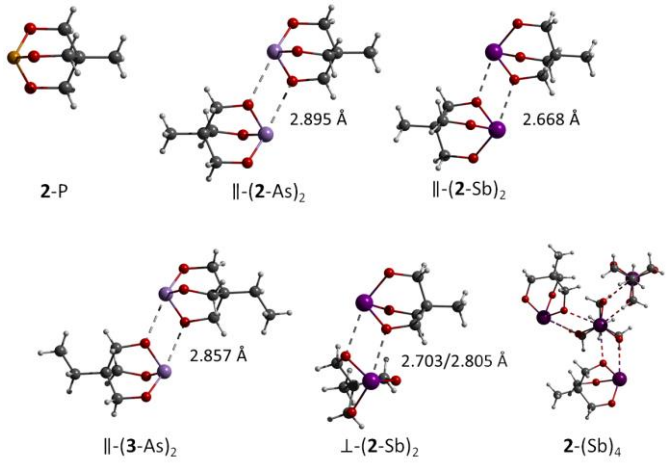

Figure 2. Ball and stick representation from crystal structures of **2**-P[40] and antiparallel dimeric units in **2**-As, **3**-As, **2**-Sb, orthogonal dimeric unit in **2**-Sb, and tetramer of **2**-Sb depicting 3 PnBs.[10]

Computational Investigation of Pnictogen Bonding

Given the similarities in electronegativities in the heavier pnictogens, and corresponding electronegativity differences with O, it could be expected that the bond polarities would be similar and therefore the strength of the pnictogen bonds would be comparable as well. Experimental evidence suggests otherwise. Density functional theory (DFT), as implemented in ORCA,[41,42] was used to provide insight into this apparent discrepancy. The geometries were optimized using the B97 exchange-correlation functional with Grimme's D3 dispersion correction.[43–46] The relativistic effects were accounted for by using a contracted all-electron basis set (def2-TZVPP)[47] with an appropriate auxiliary basis set[48] for the RI approximation and applying the zeroth-order regular approximation (ZORA). This computational level has been previously demonstrated to accurately reproduce geometric, spectroscopic and thermodynamic features in similar systems.[49,50] Maps of the ESP shown in Figure 3 reveal the fundamental differences in the tendency for the congeners to form supramolecular interactions. Immediately, the fallacy of bond polarity being the primary determiner of pnictogen bonding potential becomes

apparent. This contrasts with hydrogen bonding, where the polarity of the primary bond is the primary indicator of hydrogen bonding ability. The V_{max} associated with the region where pnictogen bonding occurs increases down the group and linear correlates with the predicted Hirshfeld charge. The electrostatic potential indicates that the pnictogen lone pair plays an important role in determining the anisotropy in the electrostatic potential around the pnictogen atom and, therefore, the directionality of the pnictogen bond.

The three V_{max} and V_{min} values at the phosphorus are negative on the 0.001 e/au surface, consistent with the nucleophilic character of these compounds.[51–56] Indeed, of the eight structurally characterized phosphorus alkoxide cages, only two examples reveal P···O contacts leading to the formation of the supramolecular synthon depicted in Figure 1.[51,57] The P···O contact distances range from 3.2-3.4 Å, close to the sum of the van der Waals radii (3.4 Å). Analysis of the 0.002 e/au electrostatic potential surface of **1**-P reveals very low, but positive, values for V_{max}. **1**-As has positive values for the three V_{max} values at the As, consistent with the formation of pnictogen bonds in the solid state structures of **2**-As and **3**-As. For **1**-Sb, the three V_{max} values at the pnictogen are more than double those of the As congener. Furthermore, each of the three values rivals those found in well-known HaB donors (F_5C_6–I: 166 kJ/mol, $(NO_2)_2C_6H_3CC$–I: 206 kJ/mol, on a 0.002 e/au isosurface),[58] suggesting the ability to form three strong interactions as is illustrated with the crystal structures of **2**-Sb and **3**-Sb. Lastly, the electrostatic potential surface for **1**-Bi reveals V_{max} values in excess of 130 kJ/mol. Furthermore, the V_{min} value is positive and larger in magnitude than the V_{max} on **1**-Sb. Despite this large and positive V_{min}, the directionality of the interaction is preserved as a result of the anisotropy of the electrostatic potential at the Bi according to the difference in the V_{max} and V_{min} values ($\Delta V_{min/max}$ in Table 2). It should be noted that this anisotropy is not well-depicted on the ESP maps in Figure 3. While the anisotropy in the ESP is not as pronounced as with the lighter congeners ($\Delta V_{min/max}$ of 45-69 kJ/mol), a difference of 21 kJ/mol should still lead to preferential, and therefore predictable binding at the V_{max} sites.

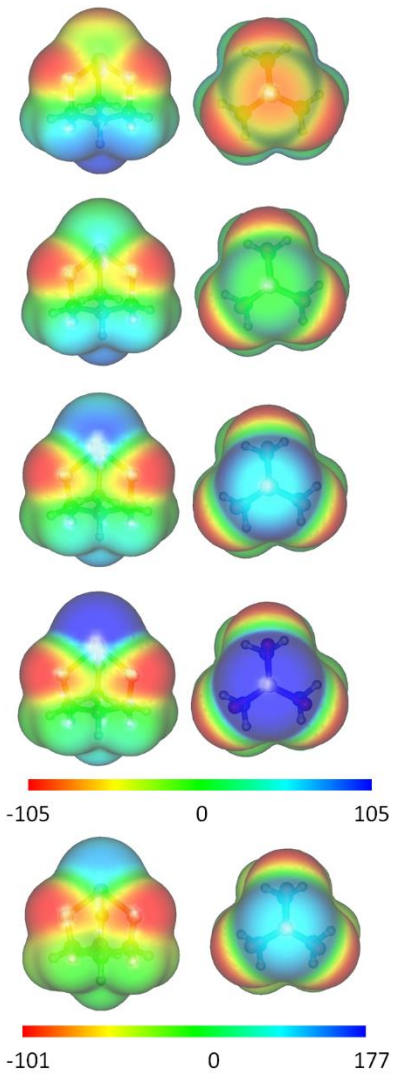

Figure 3. Side and top view of ESP of **1**-Pn mapped on the electron density (plotted at 0.001 e/au). From top to bottom: P, As, Sb, Bi (shown with two different scales). Colour scale in kJ/mol.

Table 2. DFT calculated parameters associated with monomeric **1**-Pn.

	1-P	**1**-As	**1**-Sb	**1**-Bi
x3 Pn V_{max} (kJ/mol)[c]	-16 (11)	44 (81)	96 (141)	134 (179)
Pn V_{min} (kJ/mol)[c]	-85 (-93)	-1 (6)	44 (59)	113 (139)
$\Delta V_{min/max}$ (kJ/mol)	69	45	52	21
O–Pn···V_{max} (°)	172.3	178.1	169.1	177.3
Pn Hirshfeld (Voronoi) Charge.	0.30 (0.29)	0.45 (0.41)	0.58 (0.48)	0.66 (0.55)
ρ_{Pn-O} (e/Å^3)[a]	0.165	0.149	0.122	0.113
$\nabla^2\rho_{Pn-O}$ (e/Å^5)[a]	0.463	0.337	0.408	0.330
Pn–O (Å)	1.655	1.809	1.980	2.083
O–Pn–O (°)	100.3	97.6	93.6	91.8
OOO–O–Pn (°)[b]	27.6	29.7	32.6	34.0
%Td (vs. Oh)	68	60	48	43

a) electron density and Laplacian at the bond critical point

b) centroid of the three O atoms represented with OOO

c) values correspond to the 0.001 e/au isosurface, values in parenthesis correspond to values on the 0.002 e/au isosurface

Geometry optimizations of dimers of **1**-Pn were performed to corroborate the electrostatic potential and the structural data. For **1**-P, no minimum energy geometry was found that contained P···O pnictogen bonds. Rather, weak CH···O hydrogen bonds appear to direct the mutual orientation of the two molecules. For each of **1**-As, **1**-Sb and **1**-Bi, two minimum energy supramolecular isomers that contained the $[Pn–O]_2$ supramolecular synthon were identified; a higher energy antiparallel (denoted ∥) isomer and a lower energy orthogonal (denoted ⊥) isomer. These two supramolecular isomers are consistent with what has been previously reported for anitmony.[10] The antiparallel dimer (**1**-As)$_2$ ∥ is consistent with the supramolecular arrangement in the solid state structures of **2**-As and **3**-As; the Pn···O distance is calculated to be only slighly longer than what is observed experimentally (Table 3). The experimental O-Pn···O angle (168.9° and 166.3° for **2**-As and **3**-As, respectively) are in good agreement with the angle that is calculated for antiparallel dimer of **1**-As. These angles are slightly more acute then the calculated O–As···V_{max} angle, which likely results from the formation of the supramolecular four-membered ring.

The calculated energies of dimerization are quite large for (**1**-Sb)$_2$ and (**1**-Bi)$_2$; owing in part to the fact that there are two pnictogen bonds, but also due to the large V_{max} values associated with these pnictogens which suggest a strong electrostatic attraction. The electron density ($\rho_{Pn\cdots O}$) at the bond critical point (bcp) of the pnictogen bond is a value that correlates well with bond strength and is experimentally measurable.[59–61] Here, for either the parallel or orthogonal dimers, $\rho_{Pn\cdots O}$ increases as As<Sb<Bi. This is consistent with trends observed for halogen and chalcogen bonds.[62–64] For halogen bonds involving substituted iodobenzenes, these values have been shown to range up to 0.034 e/Å^3; chalcogen bonds involving 1,2,5-chalcogenadiazoles have densities of up to 0.042 e/Å^3. The electron densities at the bcps for the pnictogen bonds in **1**-Sb and **1**-Bi are comparable with those of strong halogen and chalcogen bonds.

The crystal structures of **2**-Sb and **3**-Sb contain three pnictogen bonds to each antimony atom. In contrast, the crystal structures of **2**-As and **3**-As only contain one pnictogen bond per arsenic. This raises a question, if the interactions are strong enough to form once, then why not a second or third time? To determine the consequence of the formation of the first $[Pn–O]_2$ supramolecular synthon on the ability to form additional interactions, the charge on the pnictogens and the remaining V_{max} values were determined (Table 3). Only a small decrease in the charge on the pnictogen is calculated. The change in the V_{max} value was more significant. In the case of As, the remaining V_{max} values decreased by 23% while the V_{max} values for Sb decreased by 12% as measured on the 0.001 e/au isosurface. Interestingly, the V_{max} values predicted for Bi do not appear to be affected by the formation of the pnictogen bond. This appears consistent with the observation that only one PnB forms in the crystal structures of **2**-As or **3**-As while three PnBs form in the crystal structures of **2**-Sb or **3**-Sb. Furthermore, it implies that there is a negative cooperativity associated with pnictogen bond formation for As and Sb, preventing more than one As-centred PnB from forming in **2**-As or **3**-As. The large V_{max} values calculated in (**1**-Bi)$_2$ are consistent with the analysis of the FTIR spectroscopic data which suggests strong PnB formation in **2**-Bi and **3**-Bi as well as the insolubility of these materials.

Table 3. DFT calculated parameters associated with antiparallel (∥) or orthogonal (⊥) dimeric arrangements of **1**-Pn.

	∥ or ⊥	(**1**-As)$_2$	(**1**-Sb)$_2$	(**1**-Bi)$_2$
ΔE (kJ/mol)	∥	-50.5	-98.6	-124.1
$d_{Pn\cdots O}$ (Å)	∥	2.944	2.562	2.575
O-Pn···O (°)	∥	169.1	159.0	156.8
Pn V_{max} (kJ/mol)	∥	34	84	133
$\rho_{Pn\cdots O}$ (e/Å^3)[a]	∥	0.014	0.037	0.038
Pn Hirshfeld (Voronoi) Chg.	∥	0.45 (0.41)	0.57 (0.44)	0.66 (0.50)
ΔE (kJ/mol)	⊥	-76.2	-117.0	-142.9
$d_{Pn\cdots O}$ (Å)	⊥	2.998	2.653	2.616
O-Pn···O (°)	⊥	170.4	160.53	157.2
Pn V_{max} (kJ/mol)	⊥	32	85	133
$\rho_{Pn\cdots O}$ (e/Å^3)[a]	⊥	0.013	0.031	0.036
Pn Hirshfeld (Voronoi) Chg.	⊥	0.45 (0.41)	0.57 (0.45)	0.65 (0.51)

a) electron density at the bond critical point

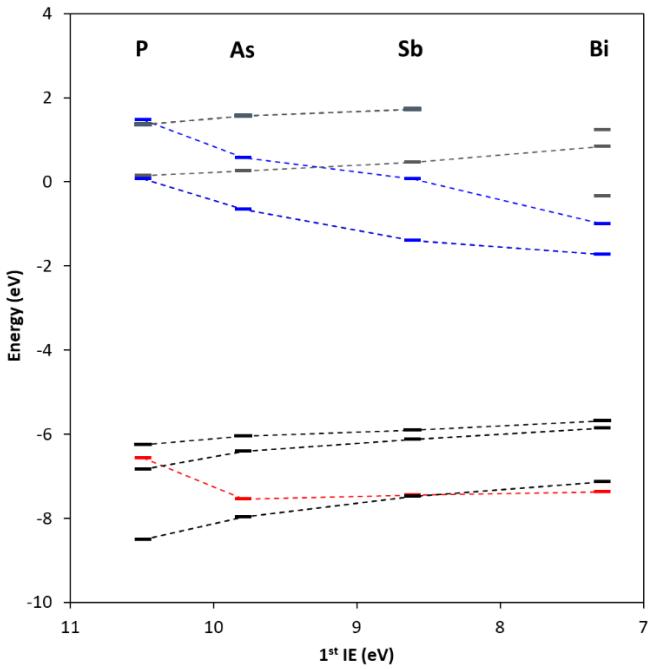

Figure 4. Kohn-Sham orbital correlation diagram for LUMO+5 to HOMO-5 of **1**-Pn. Correlated with 1st ionization energy of the pnictogen. Black/Red: Occupied, Grey/Blue: Unoccupied. Red depicts orbital with pnictogen lone-pair character, blue depicts orbitals with Pn-O σ* character.

To gain some additional insight into the origin of the increased propensity to form PnBs down the group, a variety of analysis were performed on the monomers. Inspection of the molecular orbitals for the four congeners allows for a useful conceptual model to be constructed.[65] Figure 4 depicts the frontier Kohn-Sham orbital energies of **1**-P to **1**-Bi correlated with the 1st ionization energy of the pnictogen. Most of the orbitals follow a predictable trend. The significant exception is the orbital that corresponds to the pnictogen lone pair (depicted in red in Figure 4 and visualized in Figure 5). The energy of the lone pair in **1**-P is significantly higher than in the heavier congeners. This is consistent with Lewis basic character of P in most trivalent compounds. Furthermore, the percent contribution from the pnictogen to this orbital decreases from 72% to 30% from P to Bi according to a Mulliken analysis. This trend mirrors the change that occurs in the geometry around the pnictogen. Each of the pnictogen atoms has bond angles that lay between those of an ideal tetrahedron and an ideal octahedron. By evaluating the $OOO_{centroid}$-O-Pn angle, and normalizing it over the range of tetrahedral (19.5°) and octahedral (45°), a %tetrahedral (vs. octahedral) character can be evaluated. The percent tetrahedral character decreases from P to Bi (Table 2). This change necessarily increases the s character of the lone pair, rendering it increasingly stereochemically inert. The localization of the lone pair of electrons is, therefore, primarily responsible for the repulsive region in the electrostatic potential for P and As. Accordingly, it also gives rise to the directionality of the interactions with the heavier pnictogens by enforcing an anisotropy in the electron density around the pnictogen.

Following the same orbital model, an important change can be observed in the low-lying antibonding orbitals (a degenerate pair with *e* character and an *a* character orbital) associated with the pnictogen-oxygen primary bonds. These orbitals, depicted in Figure 5 and in blue in Figure 4, decrease both in energy and separation from P to Bi. This renders the orbitals on the heavier congeners more energetically accessible for overlap with an incoming electron donor and, accordingly, does not lead to significant destabilization as they become populated. Furthermore, the *a* symmetry orbitals (LUMO+2 on **1**-Bi) points directly up and should, in principle, allow for additional binding along the molecular axis when electron repulsion from the lone pair is minimized.

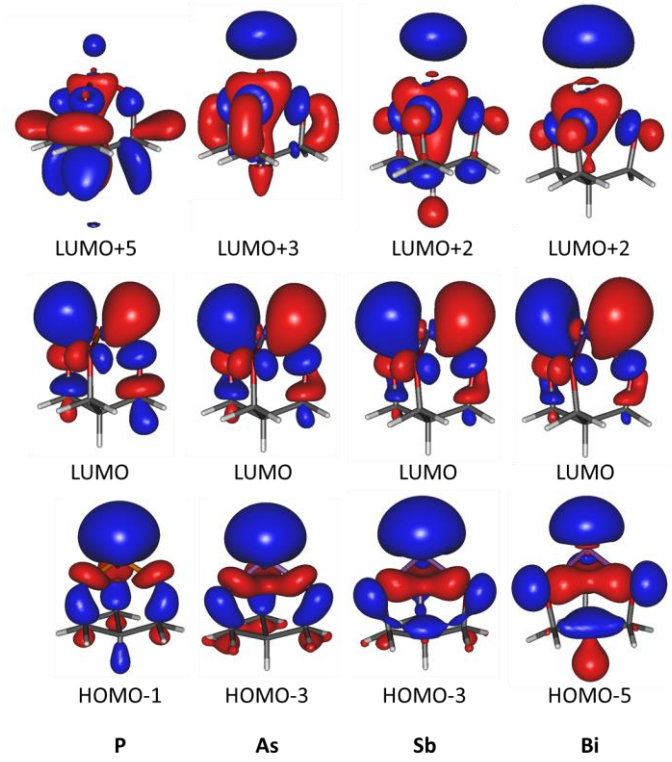

Figure 5. Kohn-Sham frontier molecular orbital representations for Pn lone pairs and Pn–O σ* in **1**-Pn (LUMO is one of a degenerate pair). All orbitals plotted as the 0.04 au isosurface.

Conclusions

Pnictogen bonding in pnictogen alkoxide cages increases in strength down the group. The P, As and Sb cages can be readily isolated and reproducibly form 0, 1 or 3 pnictogens bonds, respectively. In the case of Bi, evidence of a molecular cage was difficult to find due to the insolubility of the materials which is presumed to be the result of very strong pnictogen bonding. The strength and directionality of the pnictogen bonds results from a balance of large positive electrostatic charge on the pnictogen and the energy of the pnictogen lone pair. The energetic accessibility of the lone pair in the phosphorus cages renders the system Lewis basic. Descending the group, the lone pair becomes energetically inaccessible and helps to define the

three distinct regions of electrophilicity that lead to triple pnictogen bonding with antimony. Although three regions exist on the arsenic analogue, only single pnictogen bond is observed because the formation of the pnictogen bond results in a decreased electrophilicity at the remaining pnictogen bond sites. The negative cooperativity is observed slightly with antimony and is almost non-existent with bismuth, consistent with the shift from non-metal to metalloid to metal as the pnictogen group is descended.

Conflicts of interest

"There are no conflicts to declare".

Acknowledgements

We are grateful for research funding (CHE 1847878) and instrument support (NMR, CHE 1048553) from the National Science Foundation.

Notes and references

1. G. R. Desiraju, P. S. Ho, L. Kloo, A. C. Legon, R. Marquardt, P. Metrangolo, P. Politzer, G. Resnati and K. Rissanen, *Pure Appl. Chem.*, 2013, **85**, 1711–1713.
2. N. W. Alcock, *Adv. Inorg. Chem. Radiochem.*, 1972, **15**, 1–58.
3. O. Hassel, *Science*, 1970, **170**, 497–502.
4. H. A. Bent, *Chem. Rev.*, 1968, **68**, 587–648.
5. P. Pyykkö, *Chem. Rev.*, 1997, **97**, 597–636.
6. J. Starbuck, N. C. Norman and A. G. Orpen, *New J. Chem.*, 1999, **23**, 969–972.
7. T. G. Carter, E. R. Healey, M. A. Pitt and D. W. Johnson, *Inorg. Chem.*, 2005, **44**, 9634–9636.
8. T. G. Carter, W. J. Vickaryous, V. M. Cangelosi, D. W. Johnson, *Comments Inorg. Chem.*, 2007, **28**, 97-122.
9. W. J. Vickaryous, R. Herges and D. W. Johnson, *Ang. Chem., Int. Ed.*, 2004, **43**, 5831–5833.
10. S. Moaven, J. Yu, J. Yasin, D. K. Unruh and A. F. Cozzolino, *Inorg. Chem.*, 2017, **56**, 8372–8380.
11. C. Leroy, R. Johannson and D. L. Bryce, *J. Phys. Chem. A*, 2019, **123**, 1030-1043.
12. V. M. Cangelosi, M. A. Pitt, W. J. Vickaryous, C. A. Allen, L. N. Zakharov and D. W. Johnson, *Cryst. Growth Des.*, 2010, **10**, 3531–3536.
13. S. L. Benjamin, W. Levason, G. Reid and R. P. Warr, *Organometallics*, 2012, **31**, 1025–1034.
14. B. N. Diel, T. L. Huber and W. G. Ambacher, *Heteroat. Chem.*, 1999, **10**, 423–429.
15. K. M. Anderson, C. J. Baylies, A. H. M. M. Jahan, N. C. Norman, A. G. Orpen and J. Starbuck, *Dalton Trans.*, 2003, 3270–3277.
16. J. P. H. Charmant, A. H. M. M. Jahan, N. C. Norman, A. G. Orpen and T. J. Podesta, *Cryst. Eng. Comm.*, 2004, **6**, 29–33.
17. T. Murafuji, M. Nagasue, Y. Tashiro, Y. Sugihara and N. Azuma, *Organometallics*, 2000, **19**, 1003–1007.
18. D. Heift, R. Mokrai, J. Barrett, D. Apperley, A. Batsanov and Z. Benkő, *Chem. Eur. J.*, 2019, **25**, 4017-4024.
19. C. Silvestru, H. J. Breunig and H. Althaus, *Chem. Rev.*, 1999, **99**, 3277–3328.
20. Nekoueishahraki, P. P. Samuel, H. W. Roesky, D. Stern, J. Matussek and D. Stalke, *Organometallics*, 2012, **31**, 6697–6703.
21. G. G. Briand and N. Burford, *Adv. Inorg. Chem.*, 2000, **50**, 285–357.
22. L. Agocs, N. Burford, T. S. Cameron, J. M. Curtis, J. F. Richardson, K. N. Robertson and G. B. Yhard, *J. Am. Chem. Soc.*, 1996, **118**, 3225–3232.
23. S. L. Benjamin, W. Levason, G. Reid, M. C. Rogers and R. P. Warr, *J. Organomet. Chem.*, 2012, **708–709**, 106–111.
24. S. Moaven, J. Yu, M. Vega, D. K. Unruh and A. F. Cozzolino, *Chem. Commun.*, 2018, **54**, 8849–8852.
25. J. Qiu, D. K. Unruh and A. F. Cozzolino, *J. Phys. Chem. A*, 2016, **120**, 9257–9269.
26. J. Qiu, B. Song, X. Li and A. F. Cozzolino, *Phys. Chem. Chem. Phys.*, 2018, **20**, 46–50.
27. A. M. Christianson and F. P. Gabbaï, *Organometallics*, 2017, **36**, 3013–3015.
28. L. M. Lee, M. Tsemperouli, A. I. Poblador-Bahamonde, S. Benz, N. Sakai, K. Sugihara and S. Matile, *J. Am. Chem. Soc.*, 2019, **141**, 810-814.
29. S. Moaven, M. C. Andrews, T. J. Polaske, B. M. Karl, D. K. Unruh, E. Bosch, N. P. Bowling, A. F. Cozzolino, *J. Am. Chem. Soc.*, 2019, In Peer Review.
30. S. Benz, A. I. Poblador-Bahamonde, N. Low-Ders, S. Matile, *Ange. Chem., Int. Ed.*, 2018, **57**, 5408-5412.
31. Y. Feng, T. E. Phelps, V. Carroll, F. Gallazzi, G. Sieckman, T. J. Hoffman, C. L. Barnes, A. R. Ketring, H. M. Hennkens and S. S. Jurisson, *Dalton Trans.*, 2017, **46**, 14677–14690.
32. J. Verkade and L. Reynolds, *J. Org. Chem.*, 1960, **25**, 663–665.
33. B. A. Arbuzov, R. R. Shagidullin, V. S. Vinogradova, I. K. Shakirov and Y. M. Mareev, *Russ. Chem. Bull.*, 1980, **29**, 1270–1275.
34. B. A. Arbuzov, Y. M. Mareev, R. R. Shagidullin, V. S. Vinogradova and I. K. Shakirov, *Russ. Chem. Bull.*, 1984, **33**, 1686–1691.
35. B. A. Arbuzov, R. R. Shagidullin, V. S. Vinogradova, I. Kh. Shakirov and Yu. M. Mareev, *Russ. Chem. Bull.*, 1986, **35**, 336–342.
36. F. H. Allen, O. Kennard, D. G. Watson, L. Brammer, A. G. Orpen and R. Taylor, *J. Chem. Soc., Perkin Trans. 2*, 1987, S1–S19.
37. A. F. Cozzolino, P. J. W. Elder and I. Vargas-Baca, *Coord. Chem. Rev.*, 2011, **255**, 1426–1438.
38. A. Bondi, *J. Phys. Chem.*, 1964, **68**, 441–451.
39. S. Alvarez, *Dalton Trans.*, 2013, **42**, 8617–8636.
40. M. A. Said, B. L. Al Belewi and D. L. Hughes, *Acta Crystallogr. Sect. E, Crystallog. Comm.*, 2016, **72**, 1021–1024.
41. F. Neese, *WIREs Comput. Mol. Sci.*, 2018, **8**, e1327.
42. F. Neese, *WIREs Comput. Mol. Sci.*, 2012, **2**, 73–78.
43. S. Grimme, *J. Comput. Chem.*, 2006, **27**, 1787–1799.
44. S. Grimme, S. Ehrlich and L. Goerigk, *J. Comput. Chem.*, 2011, **32**, 1456–1465.
45. S. Grimme, J. Antony, S. Ehrlich and H. Krieg, *J. Chem. Phys.*, 2010, **132**, 154104.
46. L. Goerigk, A. Hansen, C. Bauer, S. Ehrlich, A. Najibi and S. Grimme, *Phys. Chem. Chem. Phys.*, 2017, **19**, 32184–32215.
47. F. Weigend and R. Ahlrichs, *Phys. Chem. Chem. Phys.*, 2005, **7**, 3297–3305.
48. F. Weigend, *Phys. Chem. Chem. Phys.*, 2006, **8,** 1057–1065.
49. G. E. Garrett, G. L. Gibson, R. N. Straus, D. S. Seferos and M. S. Taylor, *J. Am. Chem. Soc.*, 2015, **137**, 4126–4133.
50. G. E. Garrett, E. I. Carrera, D. S. Seferos and M. S. Taylor, *Chem. Comm.*, 2016, **52**, 9881–9884.
51. D. A. Predvoditelev, M. A. Malenkovskaya, E. V. Strebkova, K. A. Lysenko and E. E. Nifant'ev, *Russ. J. Gen. Chem.*, 2009, **79**, 49–56.
52. N. A. Foley, Z. Ke, T. B. Gunnoe, T. R. Cundari and J. L. Petersen, *Organometallics*, 2008, **27**, 3007–3017.
53. E. E. Joslin, C. L. McMullin, T. B. Gunnoe, T. R. Cundari, M. Sabat and W. H. Myers, *Inorg. Chem.*, 2012, **51**, 4791–4801.
54. K. Matsubara, T. Oda and H. Nagashima, *Organometallics*, 2001, **20**, 881–892.

55. M. Laing, M. J. Nolte, E. Singleton and E. van der Stok, *J. Organomet. Chem.*, 1978, **146**, 77–86.
56. M. A. Green, J. C. Huffman and K. G. Caulton, *J. Am. Chem. Soc.*, 1982, **104**, 2319–2320.
57. R. D. Pike and A. L. Rheingold, *Cambridge Structural Database Communication*, 2014, ILUXES.
58. C. B. Aakeröy, T. K. Wijethunga, J. Desper and M. Đaković, *Cryst. Growth Des.*, 2015, **15**, 3853–3861.
59. N. J. M. Amezaga, S. C. Pamies, N. M. Peruchena and G. L. Sosa, *J. Phys. Chem. A*, 2010, **114**, 552–562.
60. M. E. Brezgunova, J. Lieffrig, E. Aubert, S. Dahaoui, P. Fertey, S. Lebègue, J. G. Ángyán, M. Fourmigué and E. Espinosa, *Cryst. Growth Des.*, 2013, **13**, 3283–3289.
61. T. T. T. Bui, S. Dahaoui, C. Lecomte, G. R. Desiraju and E. Espinosa, *Ang. Chem. Int. Ed.*, 2009, **48**, 3838–3841.
62. N. Han, Y. Zeng, X. Li, S. Zheng and L. Meng, *J. Phys. Chem. A*, 2013, **117**, 12959–12968.
63. A. F. Cozzolino, P. J. W. Elder, L. M. Lee and I. Vargas-Baca, *Can. J. Chem.*, 2013, **91**, 338–347.
64. A. Bauzá, D. Quiñonero, A. Frontera and P. M. Deyà, *Phys. Chem. Chem. Phys.*, 2011, **13**, 20371–20379.
65. F. M. Bickelhaupt and E. J. Baerends, *Rev. comput. Chem.*, 2000, **15**, 1–86.

Antimony cages have the best balance between strength and directionality compared to the other congeners